V. Kryzhanivskyy[1, 2], V. Bushlya[1, *], O. Gutnichenko[1],
R. M'Saoubi[3], J.-E. Ståhl[1]

[1]Division of Production and Materials Engineering, Lund University,
Lund, Sweden
[2]Department of Software Development, Zhytomyr State
Technological University, Zhytomyr, Ukraine
[3]SECO Tools AB, Fagersta, Sweden
volodymyr.bushlya@iprod.lth.se

Influence of tool material and tool wear on tool temperature in hard turning reconstructed via inverse problem solution

In this work the cutting tool temperature distribution that develops during turning of hardened cold-work tool steel is modeled on the basis of experimental data. The data obtained from a series of thermocouples, placed on a PCBN insert, into an anvil, and into a toolholder, were used as the input for the model. An inverse problem was solved, where the heat fluxes were computed. The temperature distribution was modeled for the case of new tools, as well as for the case of its development in the course of a tool wear. The reconstructed temperature distributions were in good agreement with the measured data. The heat flux through rake face was found to be reducing with the decrease of thermal conductivity of the tool material.

Keywords: *tool temperature, inverse problem, PCBN.*

INTRODUCTION

The importance and necessity of a detailed study of the temperature distribution in cutting cannot be overestimated. A significant part of the energy consumed in metal cutting process manifests itself as a heat that affects the tool wear, tool life, workpiece surface integrity, etc. In fact temperature is an important phenomenon observed that links the initial machining conditions (cutting speed, feed, materials, etc.) with the result (tool wear, the quality of machined components).

On the other hand, the temperature can be readily measured with appropriate equipment or calculated with the help of boundary value problems for heat equation, yet questions of accuracy and verification are often open. Thermal studies can be divided into several sections: the temperature measurement [1–3], analytical description of the temperature distributions [4, 5], finite element modeling [6, 7] and, finally, hybrid analytical and numerical thermal modeling applied to different manufacturing processes [8–10].

The process of the temperature distribution is well described by boundary value problems for PDE used in analytical and hybrid modeling, but the boundary conditions in these problems, such as heat fluxes and heat exchange with environment, remain hard to be determined. Inverse problem solution has proven to be efficient for estimation of such the unknown boundary conditions [11–14]. Temperature is

measured in predefined points and inverse problem is iteratively solved until the measured and computed temperatures converge.

One of the features of the heat inverse problem is that it is ill-posed in Hadamar's sense [15]. The computational aspect of this fact leads to instability of iterative solution algorithms. To obtain the well-posed formulation of the inverse problem, the regularization procedure is required. It is carried out on the basis of additional information about the solution. This means that a stable solution algorithm for one inverse problem may behave differently when solving another problem meaning that no universal algorithms for solving inverse problems exist. The issue becomes more complicated in cases of 3D geometry and temperature-dependent material properties.

Alternatively an inverse problem can be solved by the method of selection [16]. For this approach, only well-posed forward heat problem is solved on each step of iterative solution algorithm. When applied to machining, this idea may be briefly formulated in the following way [17]: creation of a FE forward model of the temperature distribution where the sought parameters are variables; measurement of the temperature in predefined points in machining experiment; iterative computation for the FE model converging to measured temperatures; reconstruction of the temperature distribution in the cutting tool via direct computation of the FE model. The aim of this study is to expand this previously developed approach onto 3D nonlinear modeling case and to address the issues of the temperature distribution in hard machining with PCBN tools having different thermal properties.

EXPERIMENTAL SETUP

The experimental machining operation included dry hard turning of hardened (HRC 58) tool steel Vanadis 4E (Uddeholm Tooling). Vanadis 4E is a powder metallurgy cold work tool steel. Cutting conditions corresponded to finishing operation and were kept constant: $v_c = 200$ m/min, $f = 0.15$ mm/rev, and $a_p = 0.3$ mm. Two PcBN grades having different cBN content and therefore thermal properties were used in the tests.

At room temperature, thermal conductivity of binderless cBN (BCBN) and a cBN100 grade with TiC-based binder (SECO Tools) are 170 W/(m·K) and 44 W/(m·K), respectively [18]. Thermal conductivity and its high temperature behavior were determined by laser flash apparatus LFA 467 HT HyperFlash® (NETZSCH-Gerätebau GmbH). Specific heat at elevated temperature for both grades was determined with differential scanning calorimeter DSC 404C (NETZSCH-Gerätebau GmbH).

Chamfered round inserts RNGN090300S-01020 and a toolholder CRSNL3225P09 were used in the tests. A set of channels of 0.4×0.4 mm were cut on a precision diamond disk saw in the holder itself, in the cemented carbide anvil and in the cemented carbide clamp plate, all in the center-line direction of the toolholder. Two ∅ 0.5 mm holes were drilled in the holder, their dead-end being also located on the toolholder's center-line. Eight K-type thermocouples (TC1…TC8) were placed in the channels and holes according to the schematic drawing shown in Fig. 1.

Fine-gauge Kapton insulated thermocouples (Omega Engineering) SC-KK-K-40-1M with the wire diameters of 80 μm were used for the temperature registration in respective positions (see Fig. 1). A silver thermal paste, having $k = 25$ W/(m·K), was applied on the interfaces, with thickness of 50 to 70 μm, and was filled into the channels to ensure proper contact conditions following the recommendations [1].
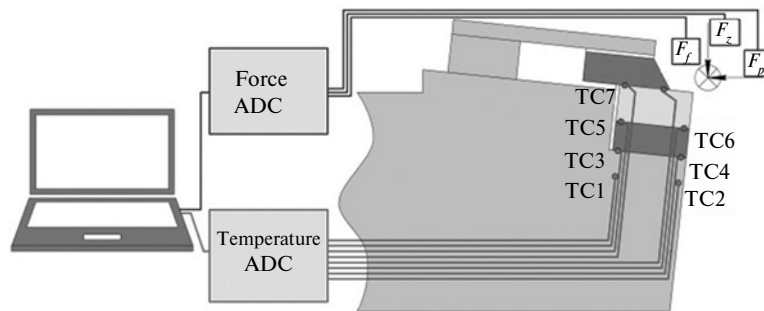
Fig. 1. Schematic view of the experimental setup.

The temperature in the cutting tool was measured during the entire tool engagement of about 200 seconds and after tool disengagement for 400 s. Cutting forces were also recorded with the help of Kistler 9129AA three-axis piezoelectric dynamometer. 3D geometrical analysis and crater measurement on the worn tools was done on the white light optical microscope InfiniteFocus Real3D, Alicona.

MODELING

Geometrically, the model is an assembly, which consists of 6 parts. The assembly (Fig. 2) was built with the SolidWorks CAD system.
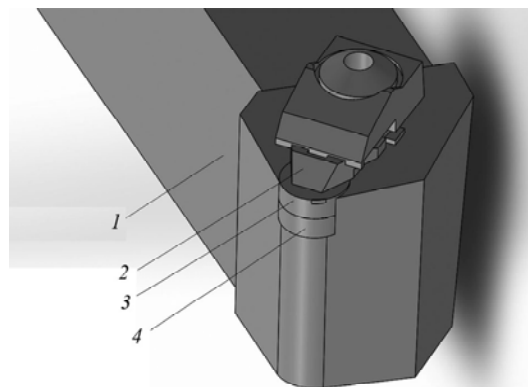

Fig. 2. CAD model of the tool in 3D: toolholder (*1*), clamp plate (*2*), insert (*3*), anvil (*4*).

It is well known that the process of the heat propagation in solids is described by the boundary value problem for the heat equation. Since the cutting tool in our experiments is an assembly of parts of different materials (Table 1), some properties of which are temperature-dependent (Figs. 3 and 4), this leads to the fact that the heat equation becomes nonlinear.

Table 1: Materials of toolholder assembly and their densities

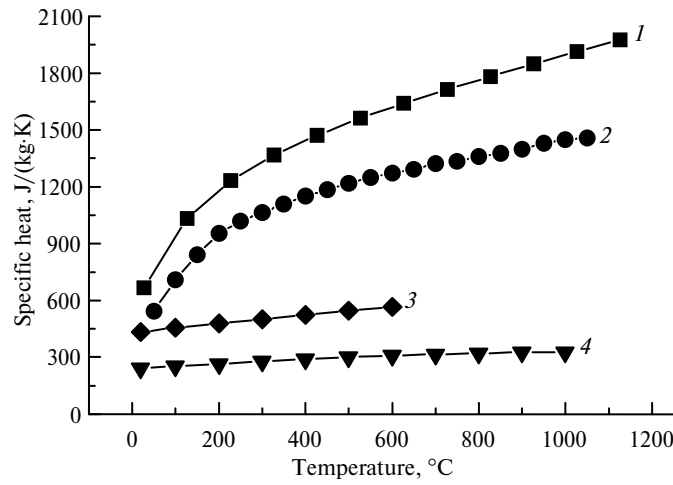| Part of the assembly	Material	Density, kg/m^3
Toolholder	Steel	7850
Anvil	WC–10Co	14600
Clamp plate	WC–10Co	14600
Insert	BCBN	3470
	cBN100	4200

Fig. 3. Temperature dependent specific heat of materials: BCBN (*1*), cBN100 (*2*), steel (*3*), WC-10Co (*4*).
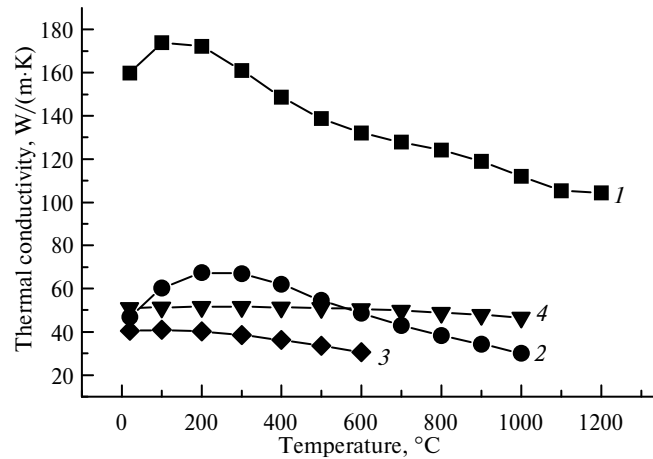

Fig. 4. Temperature dependent thermal conductivity of materials: BCBN (*1*), cBN100 (*2*), steel (*3*), WC-10Co (*4*).

Nonlinear heat equation

$$\rho_i C_{p_i}(u)\frac{\partial u_i}{\partial t} - \operatorname{div}(k_i(u)\operatorname{grad} u_i) = 0, \tag{1}$$

where i is the index of a part; ρ is the density; C_p is the specific heat; k is the thermal conductivity; t is the time; u is the temperature, expresses the law of conservation of heat for any interior point of the tool. In order to obtain its solution meeting the above cutting conditions, it is necessary to specify the boundary conditions on the boundaries of the parts.

Boundaries of parts are divided into internal and external. On the internal boundaries S_{int} of i-th and j-th parts the compatibility conditions are defined as:

$$u_i\big|_{S_{\text{int}}} = u_j\big|_{S_{\text{int}}}; \tag{2}$$

$$k_i(u)\frac{\partial}{\partial n}u_i\bigg|_{S_{int}} = k_j(u)\frac{\partial}{\partial n}u_i\bigg|_{S_{int}}, \tag{3}$$

where n is the normal to the boundary S_{int}.

Conditions of the interaction with the environment are specified at the external boundaries. In our case, the boundary contact with the chip on the rake surface A, and the contact boundary with the workpiece on the flank B (Fig. 5) are distinguished. The incoming heat fluxes q_r and q_f, respectively, are specified on these surfaces. These values are considered as unknown parameters to be determined.
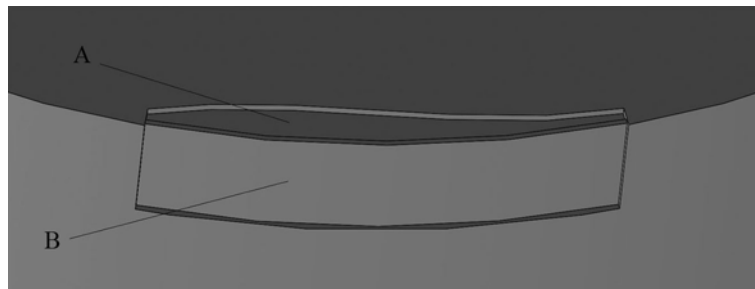

Fig. 5. Contact surfaces on rake face (A) and flank (B).

The dimensions of these contact surfaces are modelled on the basis of microscopy data (Fig. 6) for the respective worn out tools.

1 mm

Fig. 6. 3D view of worn BCBN tool.

The heat fluxes into the tool body come as a result of the heat that is released in the primary, secondary, and tertiary zones (Fig. 7) [19].

On all other external boundaries, the boundary conditions of the heat exchange with the environment are considered as follows:

$$k_i(u)\frac{\partial}{\partial n}u_i\bigg|_{S_{int}} = h_i(u_{ext} - u), \tag{4}$$

where u_{ext} is the surrounding temperature; h_i – are coefficients of heat exchange, which were taken from [17].

Due to the wear process, the contact zone B on the flank face of the tool increases linearly from the value of the edge radius $r_\beta = 20$ μm to the value $VB = 645$ μm for BCBN and $VB = 137$ μm for cBN100, both of which are deter-

mined experimentally via 3D microscopy. This flank wear process is simulated by linearly increasing the heat source area acting on the flank face (Fig. 8).
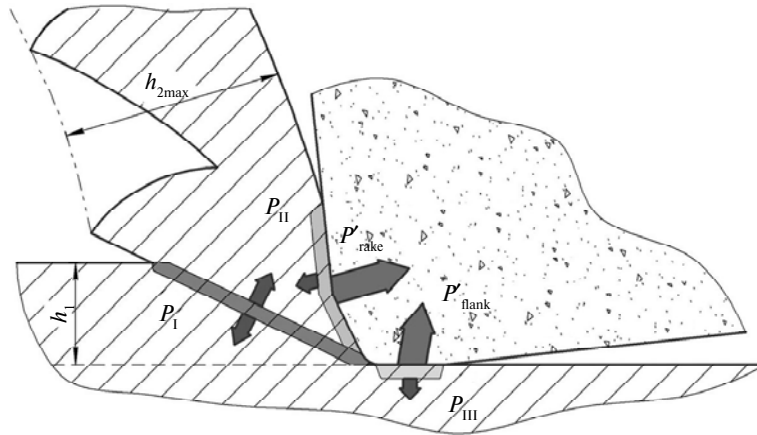

Fig. 7. Schematic representation of the zones in which heat is generated during cutting: $P'_{\text{rake}} = \eta_2 P_I + \beta_1 P_I$, $P'_{\text{flank}} = \eta_1 P_I + \varepsilon_1 P_{III}$.
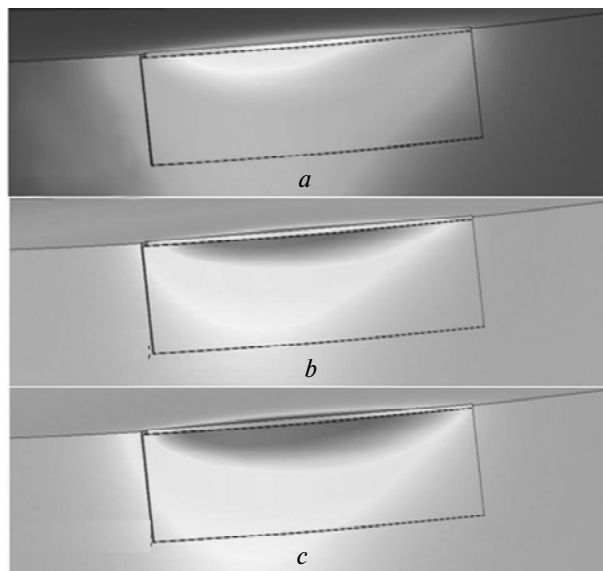

Fig. 8. Simulation of wear by enlarging heat source acting on the flank: 1 (*a*), 100 (*b*), 200 (*c*) s.

The obtained boundary value problem Eqs. (1)–(4) can be solved if the heat fluxes through the rake and flank faces are identified. The universal methods for their determination based on the cutting conditions are not known.

Therefore, an approach based on inverse problems of mathematical physics [16, 20] was used for their determination.

To obtain stable approximate solutions of the ill-posed inverse problems the additional a priori information about the behaviour of the solution of the forward problem must be used. In our case, this a priori quantitative information is the temperature measured in predefined points (see Fig. 1), where the thermocouples are installed.

www.ism.kiev.ua/stm

This makes it possible to use the approximate method of solution, the so called method of selection, for which the computation can be easily numerically performed. Its basic idea is that the elements of some predefined set M of forward problem solutions are calculated and an approximation solution is taken as an element x, which provides minimal error between the computed solution of forward problem and measured temperatures in a chosen norm.

Typically, M is a set of elements x which depend on a finite number of parameters changing in some limits so that the set M is a closed subset in a finite-dimensional vector space.

In fact, solving the inverse problem is reduced to a constrained optimization problem, where $f(x)$ should be minimized subject to some constraints. In general, the methods of its solutions are basically iterative.

In order to minimize the difference between the measured and the calculated temperatures, the objective function is established as:

$$f(q_r, q_f) = \max_{(j,t) \in I \times T} (u_j^{\text{mes}}(t) - u_j^{\text{calc}}(t, q_r, q_f))^2 \tag{5}$$

where q_r, q_f are the heat fluxes on rake and flank, respectively, j is the index of thermocouples, $I = \{1, \ldots, 8\}$ is a set of thermocouple indexes, T is the time interval of modelling, t is the time, $u_j^{\text{mes}}(t)$ is the temperature measured by the j-th thermocouple, $u_j^{\text{calc}}(t, q_r, q_f)$ is the temperature calculated at the point where the j-th thermocouple as long as q_r, q_f are given.

Next, the constraints are formulated. Obviously, the heat fluxes are limited by total power consumed during the cutting process. So, the constraints can be expressed as

$$q_r \le \frac{P}{S}, \ q_f \le \frac{P}{S}, \tag{6}$$

where P is the total power; S is the area of contact.

To be able to compute the power consumption a cutting process requires, the cutting forces parallel to the process speed directions need to be measured [19].

$$P = F_c v_c + F_f v_f + F_p v_p, \tag{7}$$

where F_c, F_f, F_p and v_c, v_f, v_p are orthogonal components of cutting force and speed, respectively.

In our case $v_c \gg v_f$, $v_p = 0$. This allows the axial and radial directions to be ignored. According to Fig. 9, the maximum cutting forces for worn tools are equal $F_c = 420$ N (BCBN) and $F_c = 243$ N (cBN100) which correspond to PBCBN = 1.4 kW and PcBN100 = 0.81 kW.

The dimensions of the contact area on rake and flank faces are estimated with the help of the microscopy. For unworn tool it equals to 0.22 mm². This provides the upper boundary of the heat flux for both rake and flank surfaces denoted as U_{BCBN} and U_{cBN100}.

In addition to the above, another boundary is the absence of negative values of heat fluxes. This fact may be represented algebraically as

$$q_r \ge 0, q_f \ge 0. \tag{8}$$

Thus, the inverse problem in the mathematical programming model is as follows:

Minimize function Eq. (5) subject to

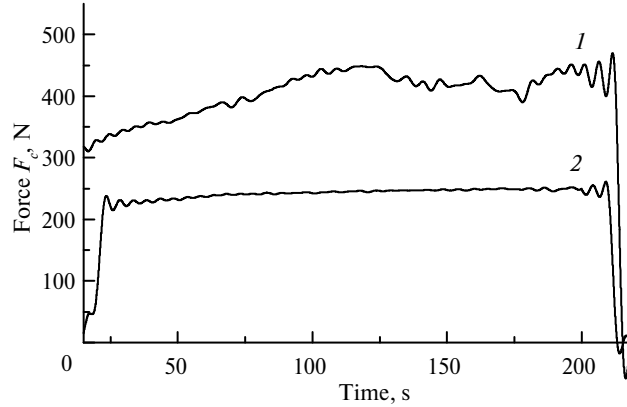$$0 \leq q_r \leq U, \; 0 \leq q_f \leq U. \tag{9}$$

Fig. 9. Forces BCBN (*1*) and cBN100 (*2*).

This problem is a constrained optimization problem with complicated objective function Eq. (5), for which differential properties are unknown and which has relatively simple constraints Eq. (9). In order to bring it to the unconstrained optimization problem a penalty function is introduced as

$$p(q_r, q_f, z) = \exp(z(q_r - U)) + \exp(z(-q_r)) + \exp(z(q_f - U)) + \exp(z(-q_f)), \tag{10}$$

where z is the iteratively increasing penalty parameter.

Because the differential properties of the function Eq. (5) are unknown a commonly applied numerical Nelder-Mead method [21] to minimize the following objective function is used

$$F(q_r, q_f, z) = f(q_r, q_f) + p(q_r, q_f, z). \tag{11}$$

Except for the finite element method of code and mesh generation tools, the model presented above have been implemented as MATLAB scripts. This implementation is modular, built around combining COMSOL Multiphysics® and MATLAB®, and has proved to be flexible and easily maintained.

COMSOL Multiphysics allowed building 3D thermal model, which was built on the basis of imported geometry from SolidWorks (see Fig. 2) and time-dependent "Heat Transfer in Solids" physics.

Interaction of scripts:

1. Inverse_problem (root) forms the set of initials points and starts iterative minimization procedure from each point. It yields the best obtained result.

2. Objective_function calls a script which solves the boundary value problem for non-linear heat equation, takes into account changing geometry and compares calculated temperatures with measured ones stored in external files. This script calculates the penalty function Eq. (10) as well.

3. Temperature_distribution creates an instance of COMSOL model class, sets appropriate attributes values and runs COMSOL solver on the COMSOL server.

RESULTS

The value of the fluxes q_r and q_f found for the conditions of function (Eq. 5) minimization are listed in Table 2. The values of the fluxes are in good agreement with the value obtained by other methods [11, 12].

www.ism.kiev.ua/stm

Table 2. Obtained heat fluxes [W/m^2]

Surface	BCBN	cBN100
Rake	3.51×10^8	1.33×10^8
Flank	1.45×10^7	1.13×10^7

The optimized value of the objective function Eq. (5), i.e. the maximum of the mismatch between the model and the experiment over the entire time of the temperature measurement for all thermocouples, ensured the maximum difference between measured and calculated temperatures up to 40 °C for both BCBN and cBN100 tools. Figures 10 and 11 show the behavior of measured and calculated temperatures for selected thermocouple data. This mismatch is most likely related to the model simplification associated with the use of constant heat fluxes over the modeling time and their uniform distribution on the contacting surfaces.
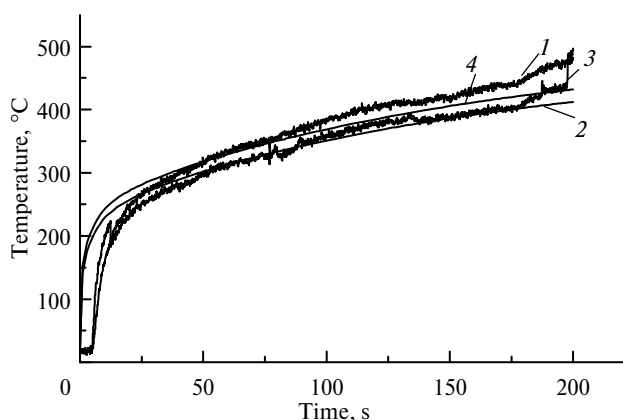

Fig. 10. Comparison of several model and experimental thermocouple readings for BCBN tool: TC10mes (*1*), TC10calc (*2*), TC8mes (*3*), TC8calc (*4*).
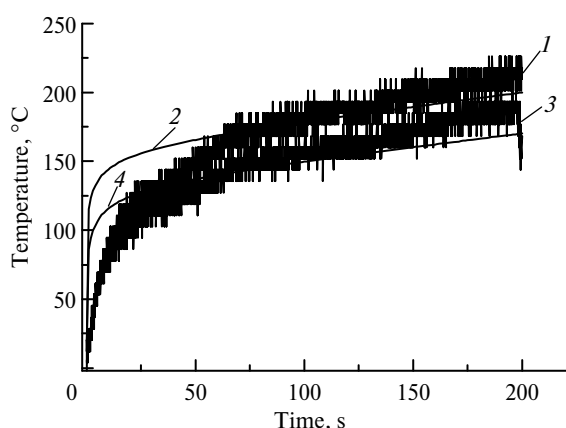

Fig. 11. Comparison of several model and experimental thermocouple readings for CBN100 tool: TC10mes (*1*), TC10calc (*2*), TC8mes (*3*), TC8calc (*4*).

It is also seen that the heat flux through the rake is lower for cBN100 than for BCBN tools. This is consistent with results of [22, 23] showing that the heat partition coefficient β_1 (see Fig. 7), i.e., the portion of the friction heat generated on the rake and transmitted into the tool, reduces with the reduced thermal

conductivity of a tool material, meaning that higher fraction of the heat will be left in a chip.

The maximum temperature developing on the tool in the course of machining and tool wear is presented in Fig. 12. It is seen that upon stabilization, within several seconds, the maximum tool temperature attains the value of $u_{max} = 680$ °C and continues to increase linearly with the tool wear progression up to $u_{max} = 940$ °C and $u_{max} = 1120$ °C for cBN100 and BCBN, correspondingly. Similar temperatures for new tools were obtained with IR-CCD technique in hard turning PM tool steels [24].
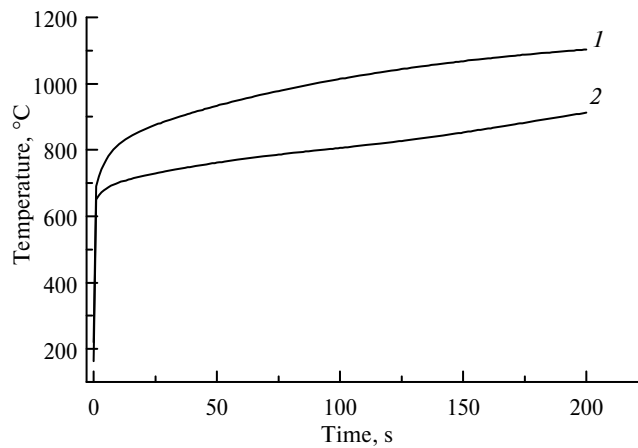

Fig. 12. Maximum temperature for BCBN (*1*) and cBN100 (*2*).

This difference in the end temperature is explained by more intensive wear of BCBN compared to cBN100, as also observed in machining Inconel 718 with the same PCBN grades [25]. Indeed, if we consider the temperature distribution in the tool at the moment of the equivalent flank wear *VB* for both tool grades, then the maximum temperature is close for both cBN100 and BCBN and equals 930–940 °C (Fig. 13).

The difference in the temperature field developing on PCBN grades having different thermal conductivity is very significant. Figure 14 shows that a more uniform temperature field is developed for BCBN grade having significantly higher thermal conductivity *k* (see Fig. 4). The maximum temperature is observed in the middle of the tool-chip contact. For cBN100 having lower *k* (see Fig. 14), the thermal gradient observed in the tool is much higher. Additionally, the maximum temperature is located closer to edge line, which should affect the depth, shape, and location of the crater developing on the tool rake.

CONCLUSIONS

The experiment consisted of finishing hard turning of cold work tool steel Vanadis 4E (HRC 59) at cutting speed $v_c = 200$ m/min. Two polycrystalline cubic boron nitride grades were tested in the respective machining case. The difference between the grades was both in their composition and their thermal properties. Data on the flank and crater wear used in the modeling were measured with the help of 3D microscopy.
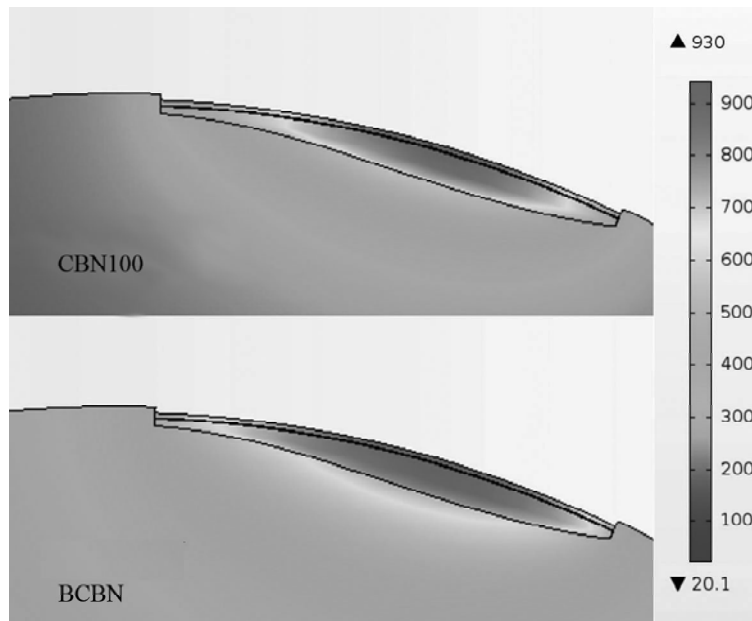
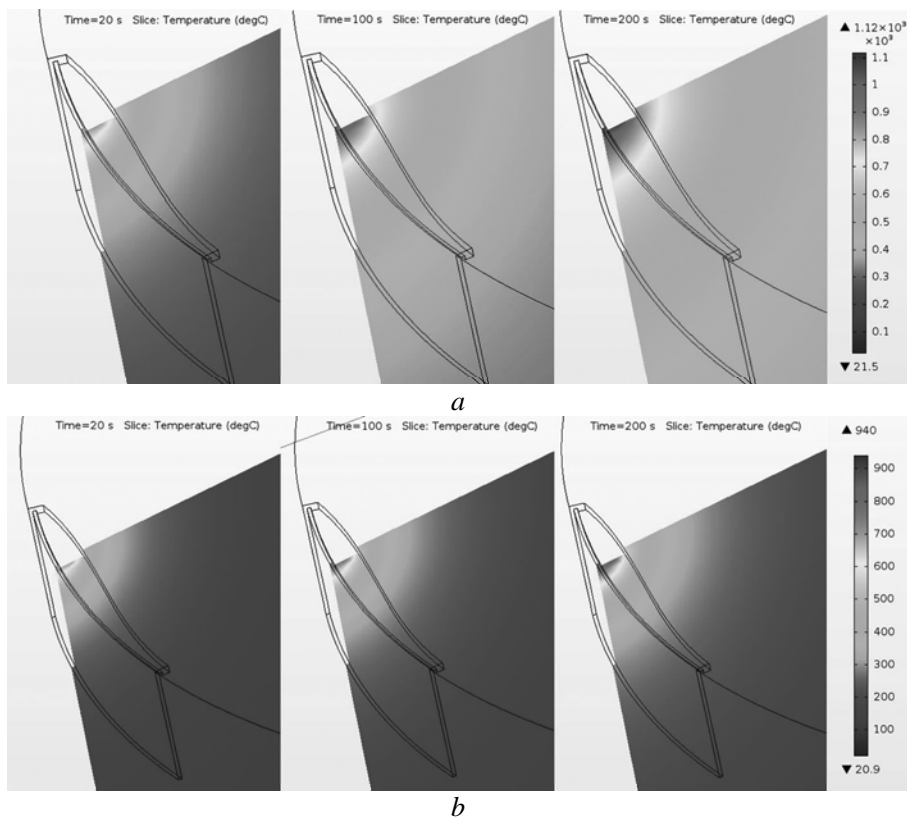Fig. 13. Temperature distributions at identical flank wear.

Fig. 14. Temperature distribution in BCBN (*a*) and cBN100 (*b*) tools at different time and wear.

According to the results presented above, the following conclusions can be drawn: novel approach based on the inverse problem solution, was developed in

order to determine the temperature distribution in the cutting tool. The model has adjustable tool geometry that allows taking into account the development of a tool wear during the machining. The solution of the ill-posed inverse problem was based on mathematical programming where the objective function (the maximum of squared difference between the computed and measured data in the points of interest) was minimized. The reconstructed temperature distributions were in good agreement with the measured data. The heat flux through rake face was reducing with the decrease of thermal conductivity of the tool.

Отримано розподіл температури різального інструменту при точінні загартованої холодно-штампованої сталі інструменту моделюванням на основі експериментальних даних. Дані, що отримано для ряду термопар, розміщених безпосередньо на пластині з ПКНБ, всередині підкладки і в державці, було використано в якості вхідних даних для моделі. Теплові потоки при різанні було отримано розв'язанням оберненої задачі. Розподіл температури в різці було отримано як для випадку нового інструменту, так і для випадку розвитку зносу інструменту в процесі зносу. Отримані розподіли температури добре узгоджуються з виміряними даними. Було виявлено, що тепловий потік через передню поверхню інструменту зменшується при зниженні теплопровідності матеріалу інструменту.

Ключові слова*: температура різання, обернена задача, ПКНБ.*

Получено распределение температуры режущего инструмента при точении закаленной холодно-штамповой стали моделированием на основе экспериментальных данных. Данные, полученные для ряда термопар, расположенных непосредственно на пластине из ПКНБ, внутри подложки и в державке, были использованы в качестве входных данных для модели. Тепловые потоки при резании были получены решением обратной задачи. Распределение температуры в резце было получено как для случая нового инструмента, так и для случая развития износа инструмента в процессе резания. Полученные распределения температур хорошо согласуются с измеренными данными. Было обнаружено, что тепловой поток через переднюю поверхность инструмента уменьшается при снижении теплопроводности материала инструмента.

Ключевые слова*: температура резания, обратная задача, ПКНБ.*

1. *Davies M. A., Ueda T., M'saoubi R. et al.* On the measurement of temperature in material removal processes // CIRP Annals – Manuf. Tech. – 2007. – **56**. – P. 581–604.
2. *Armendia M., Garay A., Villar A. et al.* High bandwidth temperature measurement in interrupted cutting of difficult to machine materials // Ibid. – 2010. – **59**. – P. 97–100.
3. *Komanduri R., Hou Z. B.* A review of the experimental techniques for the measurement of heat and temperatures generated in some manufacturing processes and tribology // Tribol. Int. – 2001. – **34**. – P. 653–682.
4. *Zhou F., Wang X., Hu Y., Ling L.* Modelling temperature of non-equidistant primary shear zone in metal cutting // Int. J. Therm. Sci. – 2013. – **73**. – P. 38–45.
5. *Karpat Y., Özel T.* Analytical and thermal modelling of high-speed machining with chamfered tools // J. Manuf. Sci. Eng. – 2008. – **130**, N 1. – P. 0110011–01100115.
6. *Yen Y.-C., Jain A., Altan T.* A finite element analysis of orthogonal machining using different tool edge geometries // J. Mater. Process. Tech. – 2004. – **146**, N 1. – P. 72–81.

7. *Özel T., Altan T.* Process simulation using finite element method – prediction of cutting forces, tool stresses and temperatures in high-speed flat end milling // Int. J. Mach. Tools Manuf. – 2000. – **40**, N 5. – P. 713–738.

8. *M'Saoubi R., Chandrasekaran H.* Experimental study and modelling of tool temperature distribution in orthogonal cutting of AISI 316L and AISI 3115 steels // Int. J. Adv. Manuf. Tech. – 2011. – **56**, N 9–12. – P. 865–877.

9. *Marinov V. R.* Hybrid analytical-numerical solution for the shear angle in orthogonal metal cutting – Part I: Theoretical foundation // Int. J. Mech. Sci. – 2001. – **43**, N 2. – P. 399–414.

10. *Tay A. A. O., Lee K. H.* Calculation of temperature distributions in machining using a hybrid finite-element-boundary-element method // J. Mater. Process.Tech. – 1992. – **29**, N 1–3. – P. 47–62.

11. *Yvonnet J., Umbrello D., Chinesta F., Micari F.* A simple inverse procedure to determine heat flux on the tool in orthogonal cutting // Int. J. Mach. Tool. Manuf. – 2006. – **46**. – P. 820–827.

12. Norouzifard V., Hamedi M. A three-dimensional heat conduction inverse procedure to investigate tool–chip thermal interaction in machining process // Int. J. Adv. Manuf. Tech. – 2014. – **74**. – P. 1637–1648.

13. *Carvalho S. R., Lima e Silva S. M. M., Machado A. R. et al.* Temperature determination at the chip–tool interface using an inverse thermal model considering the tool and tool holder // J. Mater. Process. Tech. – 2006. – **179**. – P. 97–104.

14. *Brito R. F., Carvalho S. R., Lima e Silva S. M. M. et al.* Experimental investigation of thermal aspects in a cutting tool using COMSOL and inverse problem // Appl. Therm. Eng. – 2015. – **86**. – P. 60–68.

15. *Beck J. V., Blackwell B., Clair C. R. St. Jr. et al.* Inverse heat conduction. Ill-posed problem. – New York: A Wiley-Interscience publication, 1985. – 320 p.

16. *Tikhonov A. N., Arsenin V. Y.* Solution of Ill-posed Problems. – Washington: Winston & Sons, 1977. – 379 p.

17. *Kryzhanivskyy V., Bushlya V., Gutnichenko O., Petrusha I. A., Ståhl J.-E.* Modelling and experimental investigation of cutting temperature when rough turning hardened tool steel with PCBN tools // Procedia CIRP. – 2015. – **31**. – P. 489–495.

18. Bushlya V. M., *Gutnichenko O. A., Zhou J. M., Ståhl J.-E., Gunnarsson S.* et al. Tool wear and tool life of PCBN, binderless cBN and wBN–cBN tools in continuous finish hard turning of cold work tool steel // J. Superhard Mater. – 2014. – **36**, N 1. – P. 49–60.

19. Ståhl J.-E. Metal cutting: theories and models. – Fagersta: SECO Tools, 2012. – 580 p.

20. *Orlande H. R.B., Fudym O., Maillet D., Cotta R. M.* Thermal measurements and inverse techniques. – New York: CRC Press, Taylor & Francis Group, 2011. – 589 p.

21. *Avriel M.* Nonlinear Programming: Analysis and Methods. – New-York: Dover Publishing. – 2003. – 375 p.

22. *Kagnaya T., Lazard M., Lambert L. et al.* Temperature evolution in a WC–6%Co cutting tool during turning machining: experiment and finite element simulations // WSEAS Trans. HAMT. – 2011. – **6**. – P. 71–80.

23. *Shaw M. C.* Metal cutting principles. – Oxford: Oxford University Press, 2004. – 185 p.

24. *M'Saoubi R., Lebrun J. L., Changeux B.* A new method for cutting tool temperature measurement using CCD-infrared technique: influence of tool and coating // Mach Sci Technol. – 1998. – **2**. – P. 369–382.

25. *Bushlya V., Gutnichenko O., Zhou J. et al.* Effects of cutting speed when turning age hardened Inconel 718 with PCBN tools of binderless and low-CBN grades // Mach. Sci. Technol. – 2013. – **17**, N 4. – P. 497–523.